Supporting Information

Using fluorene to lock electronically active moieties in thermally activated delayed fluorescence emitters for high-performance non-doped organic light-emitting diodes with suppressed roll-off

Lin Wu,[a] Kai Wang,*[a] Cheng Wang,[a] Xiao-Chun Fan,[a] Yi-Zhong Shi,[a] Xiang Zhang,[a] Shao-Li Zhang,[a] Jun Ye,*[b] Cai-Jun Zheng,[c] Yan-Qing Li,[a] Jia Yu,[a] Xue-Mei Ou[a] and Xiao-Hong Zhang*[a]

a. Institute of Functional Nano & Soft Materials (FUNSOM), Jiangsu Key Laboratory for Carbon-Based Functional Materials & Devices, Soochow University, Suzhou Jiangsu, 215123, P.R. China. *Email: xiaohong_zhang@suda.edu.cn; wkai@suda.edu.cn

b. School of Materials Science and Chemical Engineering, Ningbo University, Ningbo, Zhejiang, 315211, P. R. China. E-mail: yejun@nbu.edu.cn

c. School of Optoelectronic Science and Engineering, University of Electronic Science and Technology of China, Chengdu, Sichuan, 610054, P. R. China

1. General Remarks

All commercially available reagents and chemicals were used as received without further purification. Unless otherwise noted, all reactions were carried out under a nitrogen atmosphere. The solvents were dried and purified using an Innovative Technology PS-MD-5 Solvent Purification System. NMR spectra were obtained on a Bruker 400 MHz spectrometer. The ^{1}H NMR (400 MHz) chemical shifts were measured relative to $CDCl_3$ as the internal reference ($CDCl_3$: δ = 7.26 ppm). The ^{13}C NMR (100 MHz) chemical shifts were given using $CDCl_3$ as the internal standard ($CDCl_3$: δ = 77.16 ppm). High-resolution mass spectra (HRMS) were obtained with a Shimadzu LCMS-IT-TOF (ESI). Thermogravimetric analysis (TGA) curve was carried on a Perkin Elmer at a heating rate of 10 °C·min^{-1} from 50 to 550 °C under nitrogen. Differential scanning calorimetry (DSC) curve was carried on a TA DSC 2010 unit at a heating rate of 10°C·min^{-1} from 25 to 300 °C under nitrogen. The temperature of 5% weight loss was defined as the decomposition temperature (T_d). Cyclic voltammetry (CV) curve was recorded on a CHI660C electrochemistry station in DMF solution with tetrabutylammonium hexafluorophosphate (Bu_4NPF_6) as the electrolyte at a scan rate of 100 mV·s^{-1}. Ultraviolet absorption spectra were recorded on a Hitachi U-3900 spectrophotometer. PL spectra were recorded on a Hitachi F-4600 fluorescence spectrophotometer. Transient fluorescence decays were measured via the Hamamatsu C11367-03 Quantaurus-Tau fluorescence lifetime measurement system and fluorescence quantum yields were measured with a Hamamatsu C11347-11 Quantaurus-QY measurement system. Elemental analysis was recorded from Vario Micro cube elemental analyzer.

Theoretical Calculation: The orbital distributions of the highest occupied molecular orbital (HOMO) and the lowest occupied molecular orbital (LUMO) of the optimized ground state and excited state were calculated with the time-dependent density function theory (TD-DFT) using B3LYP/6-31g(d)[1, 2] basis set in Gaussian 09 program package. The lowest excited triplet state of the emitters was calculated firstly by using B3LYP/6-31g (d) basis set with UDFT. Then, the spin-density distributions (SDDs) were analyzed via multifunctional wavefunction analyzer (Multiwfn 3.7)[3] and visualized with VMD program.

2. Synthetic procedures and characterization data

2-bromo-10H-spiro[anthracene-9,9'-fluoren]-10-one (SPBP-Br) : 2-bromo-1,1'-biphenyl (2.56 g, 11 mmol) was dissolved in 60 mL dry THF in a 250 mL three-necked flask under N_2 and cooled to -78 °C under stirring and then 4.6 mL n-butyl lithium (2.4 M) was added dropwise via a syringe. After 1 h stirring, 2-bromoanthracene-9,10-dione (2.87 g, 10 mmol) dissolved in 80 mL dry THF was added dropwise over 30 min. The mixture was stirred for 1 h at -78 °C, and then was gradually warmed up to room temperature overnight. 10 mL water was added to quench the reaction and the solvent was removed under reduced pressure. The organic solid was separated, dried over anhydrous $MgSO_4$, filtered and evaporated under reduced pressure. The resulting raw product was dissolved in AcOH (80 mL) and hydrochloric acid (3 mL), and the mixture was stirred at 80 °C overnight. After cooling down, 100 mL water was added to the mixture and the product was extracted using dichloromethane (3 × 50 mL). The raw product was obtained under vacuum and was further purified by column chromatography using petroleum ether/dichloromethane (10/1, v/v) as eluent to give compound SPBP-Br as a white powder (1.99 g, 47%).^{1}H NMR (400 MHz, $CDCl_3$) δ [ppm]: 8.42 (dd, J = 8.4 Hz, 2H), 8.31 (d, J = 8.3 Hz, 1H), 7.90 (d, J = 7.9 Hz, 2H), 7.54 (dd, J = 7.5 Hz, 1H),

7.47 – 7.39 (m, 3H), 7.32 – 7.30 (m, 1H), 7.24 – 7.20 (m, 2H), 6.90 (d, J = 6.8 Hz, 2H), 6.71 (d, J = 6.7 Hz, 1H), 6.56 – 6.54 (m, 1H). HRMS (ESI$^+$): calcd for $[C_{26}H_{15}BrO + H]^+$, 424.0311; found 424.0306.

2-(9,9-diphenylacridin-10(9H)-yl)-10H-spiro[anthracene-9,9'-fluoren]-10-one (SPBP-DPAC): SPBP-Br (423 mg, 1.0 mmol), 9,9-diphenyl-9,10-dihydroacridine (400 mg, 1.2 mmol), Sodium tert-butoxide (144 mg, 1.5 mmol), Tris(dibenzylideneacetone)dipalladium (37 mg, 0.04 mmol), Tri-tert-butyl phosphine (16 mg, 0.08 mmol) were added into 30 mL dry toluene and stirred at 110°C under nitrogen overnight. The cooled mixture was filtered directly via diatomite and then solvent was removed under reduced pressure to get pale yellow solid. The crude product was further purified by column chromatography using petroleum ether/dichloromethane (4/1, v/v) as eluent to give compound SPBP-DPAC as a yellow powder (575 mg, 85%). ^{1}H NMR (400 MHz, $CDCl_3$) δ [ppm]: 8.45 – 8.43 (m, 2H), 7.80 (d, J = 7.8 Hz, 2H), 7.43-7.36 (m, 3H), 7.32 – 7.29 (m, 1H), 7.23 – 7.13 (m, 8H), 6.95 (d, J = 7.0 Hz, 2H), 6.84 – 6.73 (m, 11H), 6.62 – 6.60 (m, 1H), 6.50 (d, J = 6.5 Hz, 1H), 6.10 – 6.08 (m, 2H). ^{13}C NMR ($CDCl_3$, 100 MHz): δ (ppm) 183.6, 156.1, 151.8, 147.7, 145.6, 144.7, 141.0, 139.1, 133.8, 131.2, 130.7, 129.8, 128.7, 128.3, 127.7, 127.6, 127.1, 125.6, 125.0, 124.8, 120.8, 120.7, 119.8, 114.3, 58.1, 56.6. HRMS (ESI$^+$): calcd for $[C_{51}H_{33}NO + H]^+$, 676.8307; found 676.8310. Elemental Analysis for $C_{51}H_{33}NO$: C 90.64, H 4.92, N, 2.07, O 2.37; found: C 90.69, H 4.92, N, 2.02.

2-(10H-spiro[acridine-9,9'-fluoren]-10-yl)-10H-spiro[anthracene-9,9'-fluoren]-10-one (SPBP-SPAC) : Compound SPBP-SPAC was synthesized according to the same procedure as that of SPBP-DPAC and yellow solid was obtained in 78% yield. ^{1}H NMR (400 MHz, $CDCl_3$) δ [ppm]: 8.75 (d, J = 8.8 Hz, 1H), 8.51 – 8.49 (m, 1H), 7.84 (d, J = 7.8 Hz, 2H), 7.75 (d, J = 7.7 Hz, 2H), 7.51 (dd, J = 7.5 Hz, 1H), 7.47 – 7.43 (m, 1H), 7.42 – 7.38 (m, 2H), 7.36 – 7.32 (m, 3H), 7.25 – 7.23 (m, 4H), 7.21 – 7.20 (m, 1H), 7.18 – 7.16 (m, 1H), 7.04 (d, J = 7.0 Hz, 2H), 6.75 – 6.71 (m, 3H), 6.65 – 6.63 (m, 1H), 6.51 – 6.46 (m, 2H), 6.32 – 6.29 (m, 2H), 6.06 – 6.04 (m, 2H). ^{13}C NMR ($CDCl_3$, 100 MHz): δ (ppm) 183.5, 150.0, 146.8, 145.8, 145.4, 144.6, 141.2, 141.0, 133.7, 131.3, 130.0, 130.2, 129.8, 128.6, 128.2, 127.5, 126.7, 126.3, 124.8, 120.7, 114.5, 58.1, 56.8. HRMS (ESI$^+$): calcd for $[C_{51}H_{31}NO + H]^+$, 674.2406; found 674.2414. Elemental Analysis for $C_{51}H_{31}NO$: C 90.91, H 4.64, N, 2.08, O 2.37; found: C 90.85, H 4.70, N, 2.08.

3. Computational Data

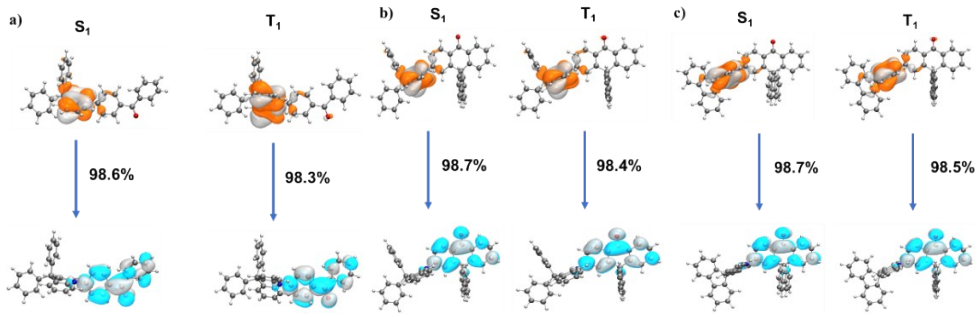

Figure S1 NTOs of singlet and triplet excited states for a) **BP-DPAC** and b) **SPBP-SPAC** and c) **SPBP-DPAC**.

Table S1. Calculated energy levels of three emitters by using 6-31G* basis set based on B3LYP optimized geometries.

Compound	S_1 [eV]	T_1 [eV]	ΔE_{ST}[a] [eV]	HOMO [eV]	LUMO [eV]
BP-DPAC	2.14	2.13	0.01	-5.15	-1.90
SPBP-DPAC	2.17	2.16	0.01	-5.08	-1.94
SPBP-SPAC	2.12	2.11	0.01	-4.96	-1.97

[a]$\Delta E_{ST} = S_1 - T_1$.

4. Crystal Data

SPBP-DPAC

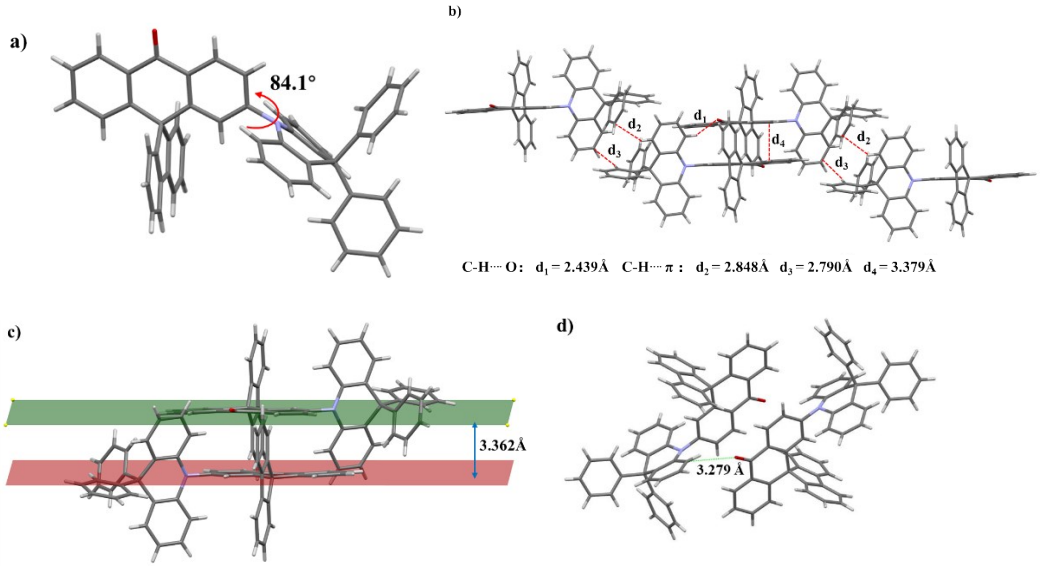

SPBP-SPAC

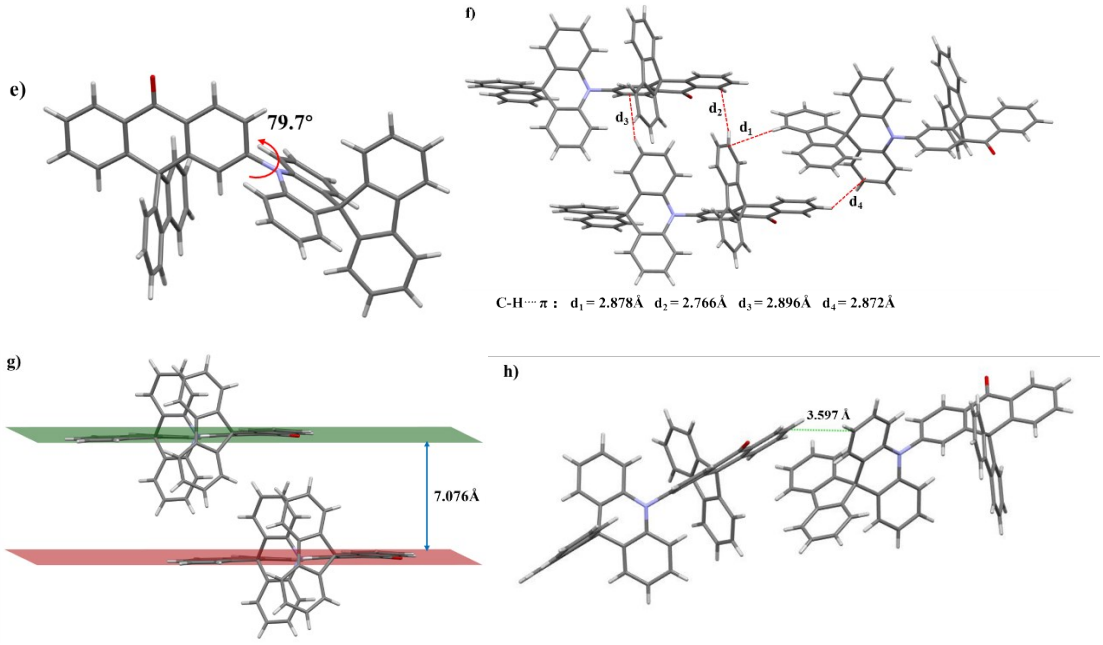

Figure S2 Information of **SPBP-DPAC** and **SPBP-SPAC** obtained from single crystals; single molecular geometries (a&e); packing patterns (b&f); identified face-to-face molecular packing distances of BP cores (c&g) and identified close intermolecular distances of electron active cores (d&h).

5. Electrochemical measurements

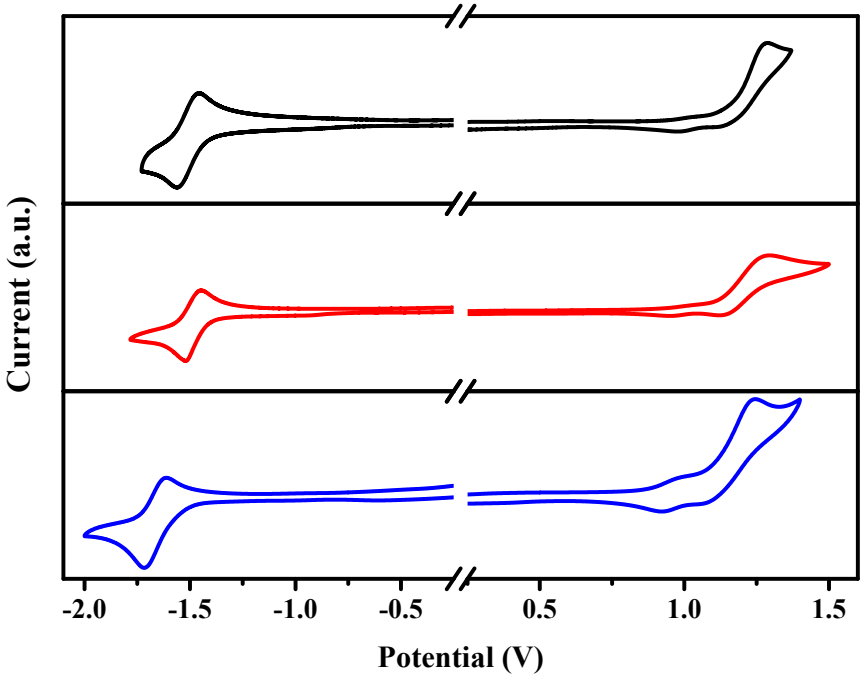

Figure S3. Cyclic voltammetry measurements of **BP-DPAC** (black), **SPBP-DPAC** (red) and **SPBP-SPAC** (blue).

6. Thermostability measurements

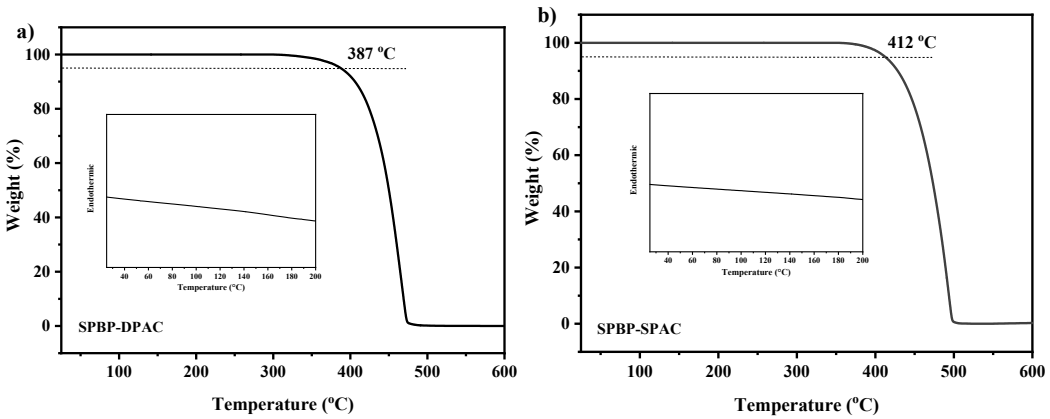

Figure S4. TGA and DSC (insert) plots of a) SPBP-DPAC and b) SPBP-SPAC.

7. Photophysical properties

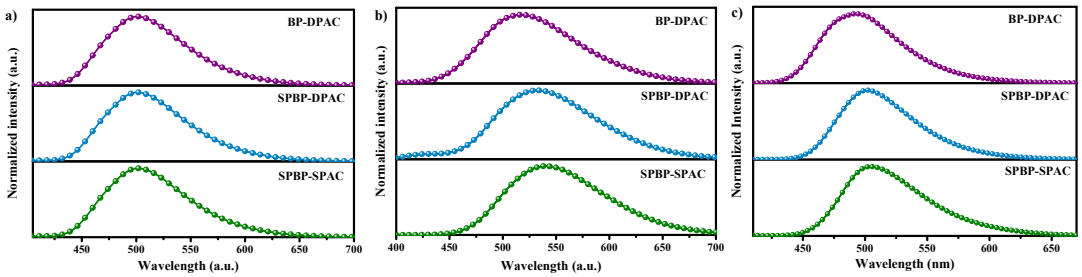

Figure S5. Normalized PL spectra of **BP-DPAC**, **SPBP-DPAC** and **SPBP-SPAC** in a) toluene, b) THF and c) neat film at room temperature.

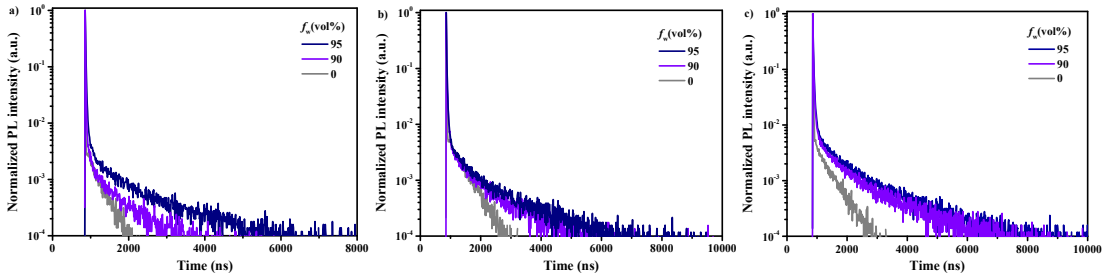

Figure S6. Transient PL decay curves of (a) **BP-DPAC** (b) **SPBP-DPAC and** (c) **SPBP-SPAC** in pure THF (grey) and in a THF/water mixture with f_w = 90% （purple） and 95% (navy blue).

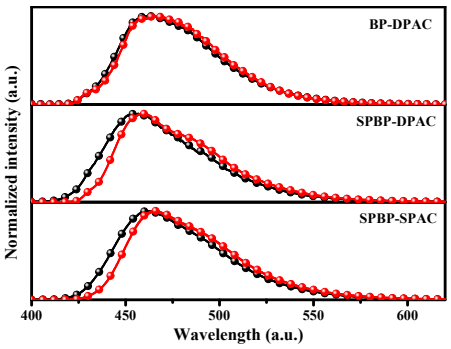

Figure S7 a) Normalized fluorescence (black) and phosphorescence (red) spectra of the studied compounds in 2-MeTHF at 77K.

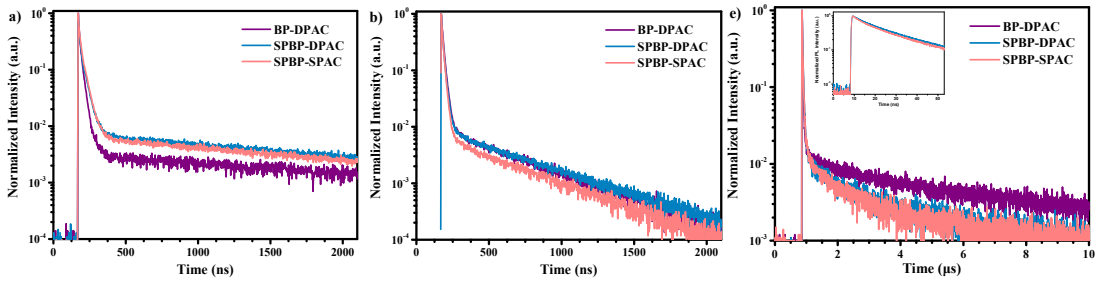

Figure S8. Transient PL characteristics of **BP-DPAC**, **SPBP-DPAC** and **SPBP-SPAC** in a) toluene, b) THF and c) their neat films under the nitrogen atmosphere at room temperature.

8. EL performance

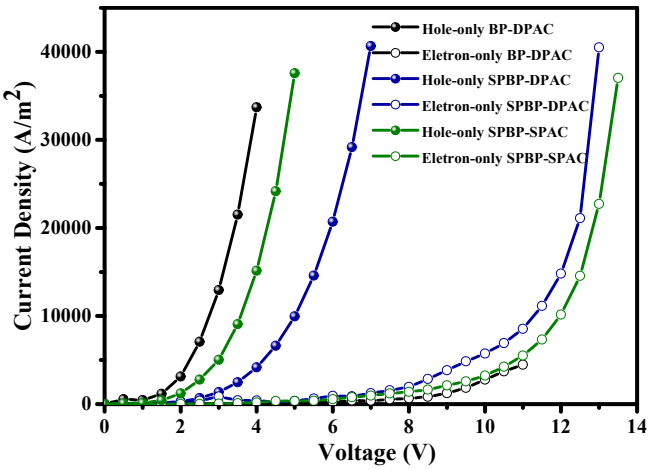

Figure S9. Current density-voltage (J-V) characteristics of hole-only device: ITO/MnO_3 (12 nm)/EML (50 nm)/ MnO_3 (10 nm)/Al, and electron-only device: ITO/Al (40 nm)/LiF (1 nm)/EML (50 nm)/LiF (1 nm)/Al.

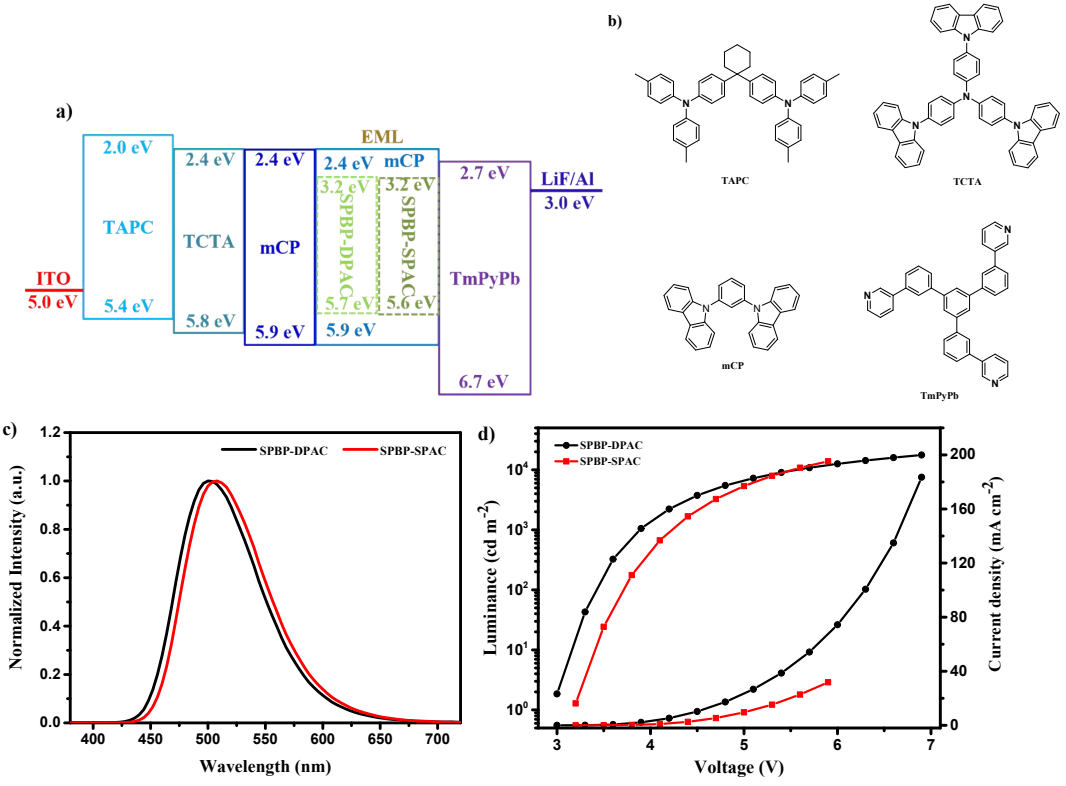

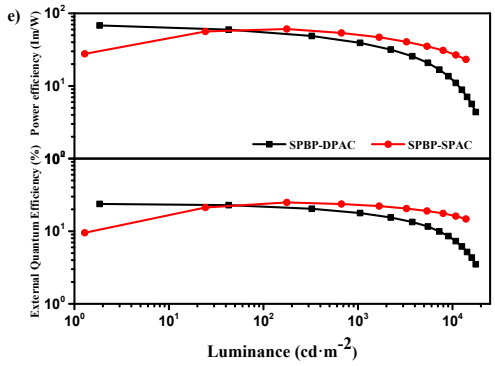

Figure S10. a) Device structures and energy level diagrams of optimized doped OLEDs; b) Molecular structures of materials used for doped OLEDs; c) EL spectra at 1000 cd m^{-2}. d) Current density and luminance versus voltage curves. e) Power efficiency and EQE versus luminance curves of doped OLEDs.

Table S2. EL performance of the doped OLEDs based on SPBP-DPAC, and SPBP-SPAC with different concentrations.

Compound	Doped C/wt%	V_{on}/V	λ_{MAX}/nm	CE/cd A^{-1}	PE/lm W^{-1}	EQE/%	CIE(x, y)
SPBP-DPAC	5	3.3	492	44.4	42.3	18.0	(0.20, 0.42)
	15	3.1	500	54.4	50.3	20.5	(0.23, 0.53)
	38	3.0	500	65.1	68.1	23.8	(0.22, 0.51)
	50	3.0	500	46.2	40.3	16.7	(0.22, 0.48)
	60	3.0	500	55.3	52.7	19.4	(0.23, 0.49)
SPBP-SPAC	8	3.3	504	61.6	53.7	22.1	(0.21, 0.47)
	18	3.2	508	73.6	60.8	24.9	(0.23, 0.53)
	33	3.0	504	64.1	55.9	22.3	(0.22, 0.51)
	50	3.2	512	68.4	61.4	22.2	(0.27, 0.55)
	71	3.2	512	68.1	61.1	22.5	(0.28, 0.55)

Table S3. EL performances of the reported sky-blue to green TADF-based high-performance non-doped OLEDs.

Ref	Emitters	λ_{EL} (nm)	CE/ PE/ EQE (cd·A^{-1}/ lm·W^{-1}/ %)		[a]$EQE_{roll\text{-}off}$ (%)	CIE (x, y)
			Maximum	@ 1000 cd·m^{-2}	@ 1000 cd·m^{-2}	
This work	**SPBP-DPAC**	**504**	**63.7/54.1/22.8**	**61.4/49.9/22.4**	**1.8**	**(0.23, 0.50)**
	SPBP-SPAC	**516**	**65.7/51.6/21.3**	**64/53.4/20.8**	**2.3**	**(0.27, 0.56)**
4	TCZPBOX	-	73.0/79.0/20.9	61.6/45.4/18.0	13.9	(0.27, 0.52)
5	2Cz-DPS	524	82.3/51.8/28.7	-/-/2.8	90.2	-
	4Cz-DPS	518	61.2/38.4/20.7	-/-/10.0	51.7	-
6	DspiroAc-TRZ	484	55.8/47.7/25.7	35.7/22.4/16.4	36.2	(0.18, 0.38)
7	DBT-BZ-DMAC	516	43.3/35.7/14.2	43.1/33.1/14.2	0.0	(0.26, 0.55)
8	DMAC-BP	510	-/-/18.9	-/-/18.0	4.8	(0.26, 0.55)
9	PTZ-XT	553	-/-/11.1	-	-	-
10	MPAc-BS	487	49.9/41.4/22.8	-/-/19.0	16.7	(0.15, 0.36)

11	TspiroS-TRZ	-	41.1/35.8/20.0	21.9/14.9/10.6	47.0	(0.16, 0.30)
12	CzDBA	560	-/-/19.0	-	-	-
13	4,4-CzSPz	526	61.2/38.4/20.7	30.2/16.0/10.3	50.2	-
14	DCB-BP-PXZ	548	72.9/81.8/22.6	-/-/22.0	2.8	(0.39,0.57)
	CBP-BP-PXZ	546	69.0/75.0/21.4	-/-/20.9	2.6	(0.39,0.57)
	mCP-BP-PXZ	542	72.3/79.0/22.1	-/-/21.5	2.9	(0.39,0.57)
	mCBP-BP-PXZ	542	70.4/76.5/21.8	-/-/21.5	1.0	(0.38,0.57)
15	CP-BZ-PXZ	554	46.1/55.7/15.3	38.4/30.2/12.7	17.0	(0.42,0.55)
	CP-BZ-PTZ	502	41.6/37.9/15.0	41.5/32.6/14.9	0.7	(0.23,0.49)
16	MeG2TAZ	510	26.5/21.5/9.4	-/-/7.1	24.5	-
	tBuG2TAZ	510	25.4/16.1/9.5	-/-/7.3	23.2	-
	PhG2TAZ	510	23.1/17.3/8.2	-/-/6.0	26.8	-
17	2CzSO	516	-/-/0.7	-	-	-
	3CzSO	528	-/-/7.3	-	-	-
18	PAPCC	521	41.8/37.1/12.6	-	-	(0.30,0.59)
	PAPTC	508	3.6/3.7/1.3	-	-	(0.25,0.47)
19	PABPC0.5	-	36.2/339/10.7	28.8/19.6/8.5	20.6	(0.36, 0.57)
	PABPC1	-	52.3/53.5/15.4	48.2/38.9/14.2	7.8	(0.36, 0.57)
	PABPC5	-	60.5/61.2/18.1	59.4/50.4/17.8	1.6	(0.40, 0.56)
	PABPC10	-	55.1/54.4/16.2	54.5/42.8/16.0	1.2	(0.40, 0.56)
20	DMAC-BPI	508	-/59.7/24.7	-/46/21.7	12.2	(0.24, 0.49)
21	DMAC-o-TRZ	504	39.3/37.0/14.7	30.0/21.2/11.3	23.1	(0.22, 0.45)
22	oTE-DRZ	524	67.4/62.3/20.6	-	-	(0.31, 0.57)
23	DMAC-TRZ	501	40.2/32.3/14.7	26.9/14.4/9.8	33.3	(0.22, 0.49)
24	B-oTC	474	37.3/27.6/19.1	19.1/17.0/9.7	49.2	(0.15, 0.26)
25	DMAc-DPS	480	-/-/19.5	-/-/14.6	25.1	(0.16, 0.29)
11	SpiroAc-TRZ	-	36.1/32.3/15.4	19.4/12.6/8.2	46.8	(0.19, 0.42)

[a] $EQE_{roll\text{-}off} = (EQE_{max}-EQE_{1000})/EQE_{max}$

9. Copies of NMR spectra

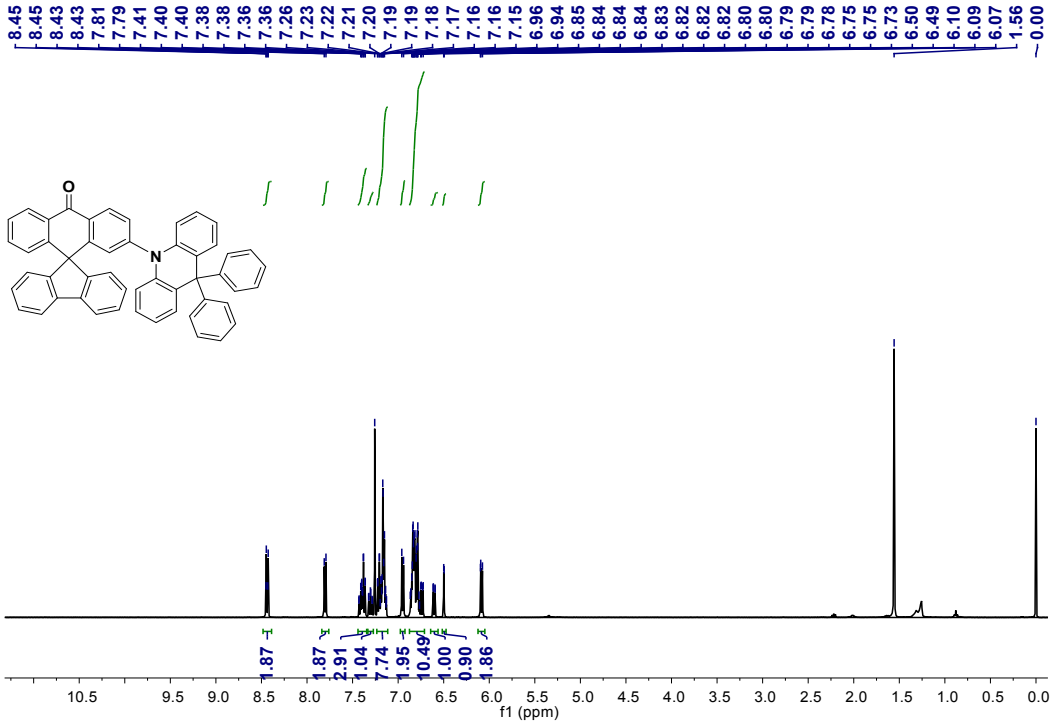

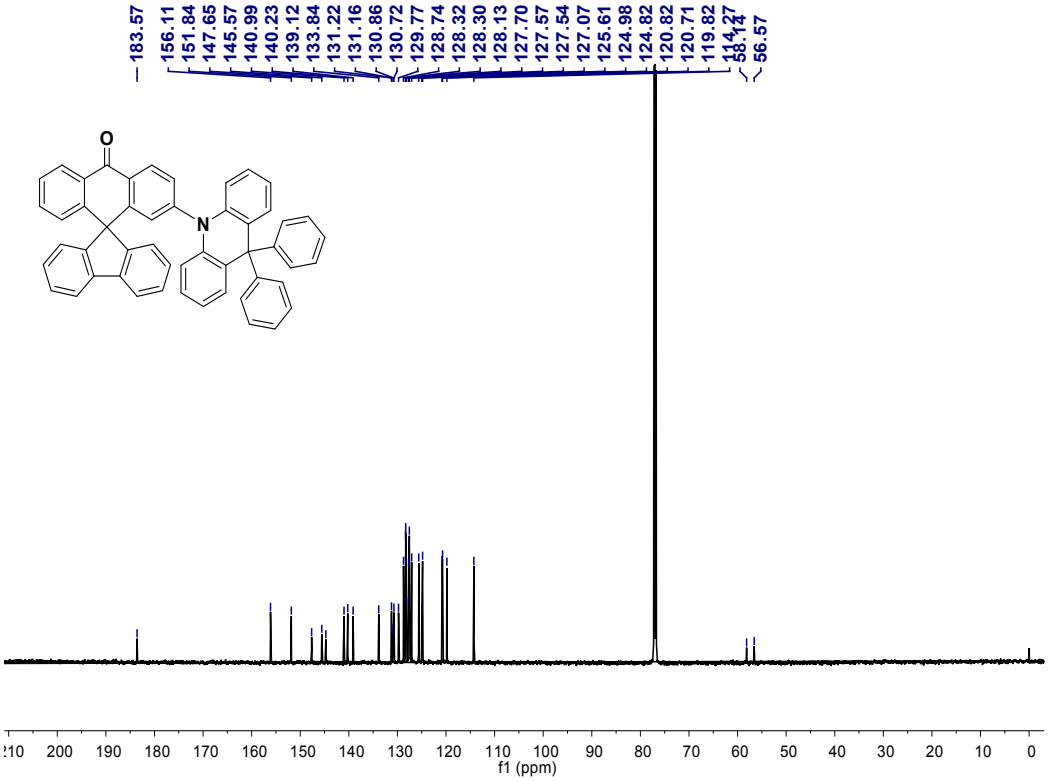

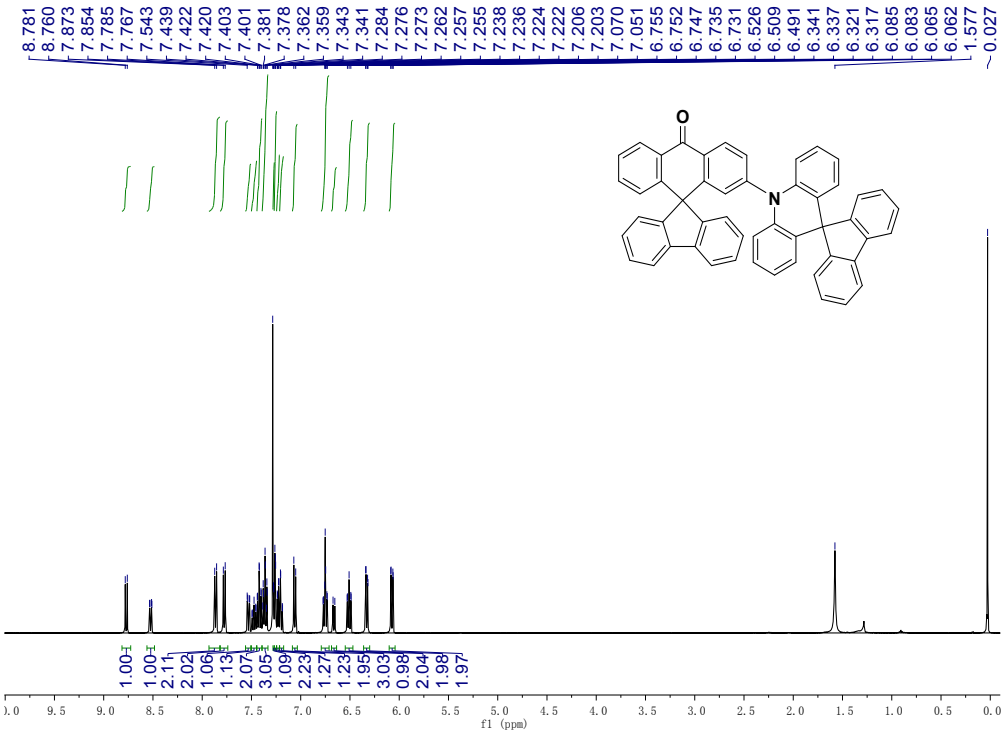

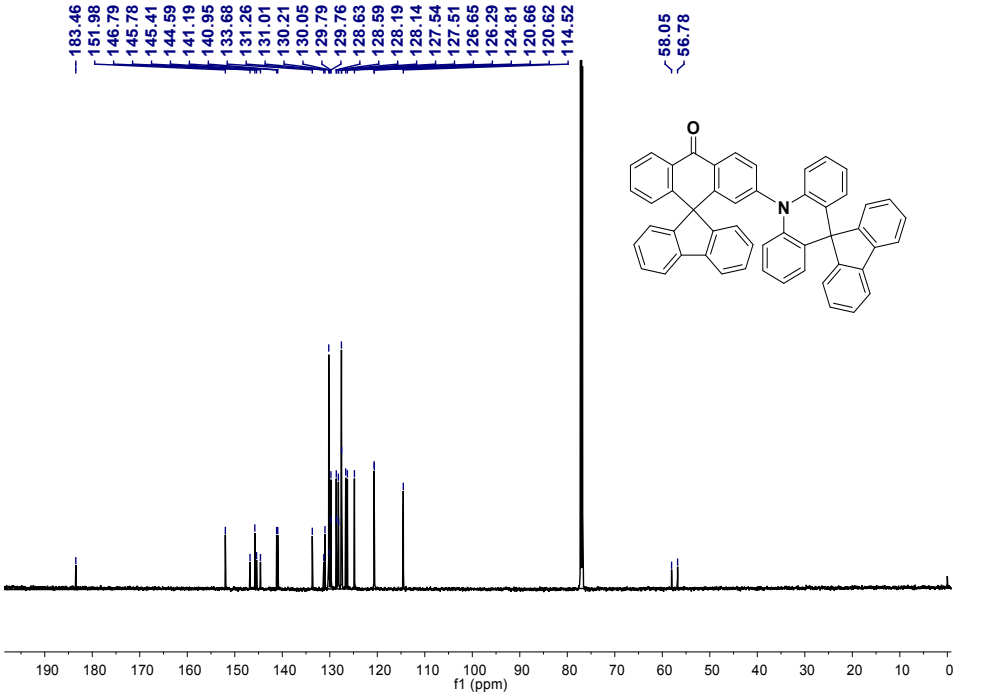

9. Reference

1. A. D. Becke, *J. Chem. Phys.*, 1993, **98**, 5648-5652.
2. P. J. Stephens, F. J. Devlin, C. F. Chabalowski and M. J. Frisch, *J. of Phys. Chem.*, 1994, **98**, 11623-11627.
3. T. Lu and F. Chen, *J. Comput. Chem.*, 2012, **33**, 580-592.
4. X. Zhang, M. W. Cooper, Y. Zhang, C. Fuentes-Hernandez, S. Barlow, S. R. Marder and B. Kippelen, *ACS Appl. Mater. Interfaces*, 2019, **11**, 12693-12698.
5. Z. Yang, Z. Mao, C. Xu, X. Chen, J. Zhao, Z. Yang, Y. Zhang, W. Wu, S. Jiao, Y. Liu, M. P.

Aldred and Z. Chi, *Chem. Sci.*, 2019, **10**, 8129-8134.
6. W. Li, W. Li, L. Gan, M. Li, N. Zheng, C. Ning, D. Chen, Y. C. Wu and S. J. Su, *ACS Appl. Mater. Interfaces*, 2020, **12**, 2717-2723.
7. J. Guo, X.-L. Li, H. Nie, W. Luo, S. Gan, S. Hu, R. Hu, A. Qin, Z. Zhao, S.-J. Su and B. Z. Tang, *Adv. Funct. Mater.*, 2017, **27**, 1606458
8. Q. Zhang, D. Tsang, H. Kuwabara, Y. Hatae, B. Li, T. Takahashi, S. Y. Lee, T. Yasuda and C. Adachi, *Adv. Mater.*, 2015, **27**, 2096-2100.
9. N. Aizawa, C.-J. Tsou, I. S. Park and T. Yasuda, *Polym J*, 2016, **49**, 197-202.
10. I. S. Park, K. Matsuo, N. Aizawa and T. Yasuda, *Adv. Funct. Mater.*, 2018, **28**, 1802031.
11. W. Li, B. Li, X. Cai, L. Gan, Z. Xu, W. Li, K. Liu, D. Chen and S. J. Su, *Angew. Chem. Int. Ed.*, 2019, **58**, 11301-11305.
12. N. B. Kotadiya, P. W. M. Blom and G.-J. A. H. Wetzelaer, *Nat. Photon.*, 2019, **13**, 765-769.
13. J. Zhao, X. Chen, Z. Yang, T. Liu, Z. Yang, Y. Zhang, J. Xu and Z. Chi, *J. Phys. Chem. C*, 2019, **123**, 1015-1020.
14. H. Liu, J. Zeng, J. Guo, H. Nie, Z. Zhao and B. Z. Tang, *Angew. Chem. Int. Ed.*, 2018, **57**, 9290-9294.
15. J. Huang, H. Nie, J. Zeng, Z. Zhuang, S. Gan, Y. Cai, J. Guo, S. J. Su, Z. Zhao and B. Z. Tang, *Angew. Chem. Int. Ed.*, 2017, **56**, 12971-12976.
16. K. Albrecht, K. Matsuoka, D. Yokoyama, Y. Sakai, A. Nakayama, K. Fujita and K. Yamamoto, *Chem. Commun.*, 2017, **53**, 2439-2442.
17. Y. Li, T. Chen, M. Huang, y. gu, S. Gong, G. Xie and C. Yang, *J. Mater. Chem. C*, 2017, **5**, 3480-3487
18. Y. Zhu, Y. Zhang, B. Yao, Y. Wang, Z. Zhang, H. Zhan, B. Zhang, Z. Xie, Y. Wang and Y. Cheng, *Macromolecules*, 2016, **49**, 4373-4377.
19. Y. Yang, S. Wang, Y. Zhu, Y. Wang, H. Zhan and Y. Cheng, *Adv. Funct. Mater.*, 2018, **28**, 1706916
20. Z. Huang, Z. Bin, R. Su, F. Yang, J. Lan and J. You, *Angew. Chem. Int. Ed.*, 2020, **59**, 9992-9996.
21. Y. Z. Shi, K. Wang, X. Li, G. L. Dai, W. Liu, K. Ke, M. Zhang, S. L. Tao, C. J. Zheng, X. M. Ou and X. H. Zhang, *Angew. Chem. Int. Ed.*, 2018, **57**, 9480-9484.
22. X. Cai, Z. Qiao, M. Li, X. Wu, Y. He, X. Jiang, Y. Cao and S. J. Su, *Angew. Chem. Int. Ed.*, 2019, **58**, 13522-13531.
23. W. Li, X. Cai, B. Li, L. Gan, Y. He, K. Liu, D. Chen, Y. C. Wu and S. J. Su, *Angew. Chem. Int. Ed.*, 2019, **58**, 582-586.
24. X. L. Chen, J. H. Jia, R. Yu, J. Z. Liao, M. X. Yang and C. Z. Lu, *Angew. Chem. Int. Ed.*, 2017, **56**, 15006-15009.
25. Q. Zhang, D. Tsang, H. Kuwabara, Y. Hatae, B. Li, T. Takahashi, S. Y. Lee, T. Yasuda and C. Adachi, *Adv. Mater.*, 2015, **27**, 2096-2100.